Numerical simulation of heat transfer properties of large-sized biomass particles during pyrolysis process

Fei-yang Han [a], Meng Wang [a], Xiao-bo Ma [a,b], Li-jie Yin [a,b,*], De-zhen Chen [a,b], Ze-qing Liu [c], Rui-na Zhang [c]

[a] Thermal & Environmental Engineering Institute, Tongji University, Shanghai 200092, China
[b] Shanghai Engineering Research Center of Multi-source Solid Wastes Co-processing and Energy Utilization, Shanghai 200092, China
[c] Shanghai Environmental Sanitation Engineering Design Institute Co., Ltd, Shanghai 200232, China

ARTICLE INFO

ABSTRACT

During the pyrolysis process of large particles, the conduction between particles cannot be ignored. In the present work, a numerical simulation model for the pyrolysis of biomass particles was established, which takes into account the conduction within the particles. Based on this model, the temperature distribution inside the particle during the pyrolysis process was determined and the effects of particle size, moisture content, and gas velocity on heat transfer characteristics were analyzed. The results showed that the temperatures at different positions of the particles along the inflow direction were quite different, and the maximum temperature difference inside the particles was about 146.7 K for a particle diameter of 10 mm and a velocity of 0.2 m/s. During the pyrolysis process of biomass particles, there were two peaks of Nusselt number. The increase of moisture content prolonged the pyrolysis time. The pyrolysis.

time of particles with moisture content of 15 % was about 1.5 times longer than that of dry particles when the particle diameter was 10 mm. Increasing the particle size decreased the difference between the two peaks and increased the time interval between the two peaks. Increasing the gas velocity can improve the heat transfer, but the effect of too high gas velocity on improving the heat transfer is limited. The present study is of great importance for a detailed understanding of the pyrolysis process of biomass particles.

1. Introduction

Excessive emission of greenhouse gasses leads to global warming. Biomass has a good potential to replace energy from conventional sources [1]. In general, biomass includes forest wastes, municipal solid wastes, specially cultivated grasses, microalgae, food wastes, and many others [2]. Biomass can provide heat through direct combustion. Biomass can provide energy and is a source of chemicals. Biomass as a carbon-neutral and renewable energy source utilization can reduce the amount of biomass that needs to be disposed of in the end and is an indispensable way to achieve the "double carbon" goal [3,4]. In this paper, biomass particles refer to wood particles, including lignin, cellulose and hemicellulose.

Pyrolysis constitutes a pivotal thermal conversion process in the realm of direct combustion, gasification, and rapid pyrolysis of solid biomass materials [5], which is one of the most important methods of biomass utilization. Compared to incineration, pyrolysis

---

reduces the production of toxic compounds such as nitrogen oxides and sulfur oxides [6]. During the pyrolysis process, biomass must be broken down into particles. Biomass particles range in size, from hundreds of microns to several centimeters [7,8]. Biomass is a poor conductor of heat with low thermal conductivity in the range of 0.21–0.71 W/(m·K) [9]. In most reactor-scale simulations, biomass particles are treated as isothermal spheres. The error introduced by this simplification is not negligible for large particles, since the slow conduction within the particles leads to a lower temperature at the center of the particles [10]. For biomass particles within the thermally-thick regime, different conversion rates occur within the biomass particle [11], and the effects of heat conduction within the particles on the heat transfer properties and volatile devolatilization need to be thoroughly considered to obtain a more accurate understanding of the reaction mechanism.

During the actual pyrolysis process of biomass particles, heat conduction occurs between particles and particles-wall, while heat convection occurs between particles and the gas in the reactor [12,13]. In simulations of biomass particle pyrolysis processes, a simplified model based on the lumped parameter method was usually used to calculate the temperature change, assuming that the heat conduction resistance of particles is much smaller than the thermal resistance of convective heat transfer and the temperature change of particles depends only on time, which is commonly known as the 0- dimensional model [14], and the effect of intra-particle conduction can be evaluated with dimensionless numbers such as Biot number (Bi). If Bi < 0.1, the distributions within the particles can be ignored. However, in the actual reaction process, the Biot number is much higher than the limit for thermally thin particles of about 0.1, and there is an obvious temperature gradient within large particles [15–17]. Therefore, different reaction processes occur simultaneously in different spatial zones of the particle, which cannot be modelled by the lumped method [18]. At the same time, during the pyrolysis process, the volatiles generated by pyrolysis leave the particle surface and generate a Stephen flow, which also affects the heat transfer efficiency between the particle surface and the surrounding gas.

Due to the fact that the 0-dimensional model is only suitable for cases with small Bi < 1 [19], one-dimensional model was developed to predict the effect of heat conduction between particles on heat transfer efficiency. The one-dimensional model considers only the radial temperature gradient in the particles, which is efficient and accurate for spherical particles and is a good approximation for long cylinders [20]. Li et al. [21] used the drying, pyrolysis, carbon and ash layers to represent the changes of wet wood, dry wood, carbon residue and ash, respectively during the pyrolysis process for drying and degassing of biomass particles. Considering a one-dimensional radiant heat flux, Blasi [9] studied the pyrolysis process of wood particles under radiant heating conditions , Wardach-Święcicka and Kardaś [22] studied the thermal behavior of a single solid particle pyrolyzing in a hot gas flow. Although the one-dimensional model can provide spatial temperature variations in the particles, transport processes inside the particles and the coupling of internal and external flow fields are usually not considered. Assuming that the shape of the particles remains unchanged, Janse et al. [23] studied the pyrolysis of particles with cylindrical, spherical and other shapes. In fact, experimental and theoretical studies indicate that the shape and size of the particles change and that the density of the biomass, species, or heating method also affects the dynamics of the biomass particles, including drying, heating rate, reaction rate and pyrolysis products [24,25].

In summary, for large-diameter biomass particles, the currently established single particle model cannot simultaneously consider the complex heterogeneous reaction process of internal and external heat transfer resistance, pyrolysis characteristics of different components within the particles, and deformation caused by different reaction rates within the particles. The accuracy of the biomass particle pyrolysis process model prediction needs to be further improved.

In the present work, a numerical simulation model for the pyrolysis of three-dimensional single-particle materials was built based on the open-source OpenFOAM® (Open Field Operation and Manipulation) software, taking into account intra-particle conduction and migration of the reaction interface during the pyrolysis process. The effect of intra-particle conduction on the overall heat transfer was analyzed, and the effect of particle size and moisture content on heat transfer properties was investigated. The present study is of great significance for the detailed understanding of the biomass particle pyrolysis process and for providing a practical technical guide.

2. Mathematical model

2.1. Conservation equation in porous media region

During the calculation process, particles are composed of cells, chemicals, lignin, charcoal, and water, and each component is evenly mixed together. As the temperature of the particles increases, water begins to evaporate. When the temperature of the particles reaches the pyrolysis temperature of each organic component, the organic component begins to decompose and generate volatile. During the pyrolysis process and with the degassing of the volatiles, the charcoal forms outside the particle. The particle refers to the unreacted area inside the particle and the porous char zone on the particle surface after the reaction. Water vapor generated by water evaporation and volatile generated by pyrolysis of organic components diffused outward through the porous medium area on the surface of particles, and further diffuse to the space outside the particles.

As the pyrolysis reaction progresses, the water and organic components in the particles are converted into vaper and volatile, resulting in a decrease in the mass and volume of the particles. The mass conservation equation for solid particles is expressed as follows:

$$-\partial_t(\varepsilon_s \rho_s) = \sum_{i \in [1, N_p]} \varepsilon_{si} \rho_s \partial_t \chi_i \tag{1}$$

$$\varepsilon_s = \sum_{i \in [1, N_s]} \varepsilon_{si} \tag{2}$$

$$\rho_s = \frac{\sum_{i \in [1,N_s]} \varepsilon_{si} \rho_{si}}{\varepsilon_s} \tag{3}$$

where ε_{si} and χ_i denote, respectively, the volume fraction and the ratio of reaction mass to initial mass of component i. During the simulation process, the change in particle size was achieved through dynamic mesh technology.

The energy conservation equation for the particle region, including the heat conduction for the inner unreacted zone and the outer porous char region, the energy change of the gas in the porous char region, and the heat transfer between the solid particle and the gas flowing through the particle surface. The energy conservation equation for the particle region is expressed as follows:

$$\sum_{i \in [1,N_p]} \left[(\varepsilon_{si}\rho_s c_{p,i}) \partial_t T_s \right] = \partial_{\mathbf{x}} \cdot (\lambda_s \partial_{\mathbf{x}} T_s) - \sum_{i \in [1,N_p]} [h_{si} \partial_t (\varepsilon_{si}\rho_s)] - \partial_t (\varepsilon_g \rho_g e_g)$$
$$+ \partial_{\mathbf{x}} \cdot \left(\sum_{j \in [1,N_g]} \varepsilon_{gj} \rho_g h_{gj} \boldsymbol{u_g} \right) + \partial_{\mathbf{x}} \cdot \sum_{j \in [1,N_g]} (Q_{gj}) + \mu \varepsilon_g^2 \left(\underline{\underline{\mathbf{K}}}^{-1} \cdot \boldsymbol{u_g} \right) \cdot \boldsymbol{u_g} + q_{gp} \tag{4}$$

$$\varepsilon_g = \sum_{j \in [1,N_g]} \varepsilon_{gj} \tag{5}$$

$$\rho_g = \frac{\sum_{j \in [1,N_g]} \varepsilon_{gj} \rho_{gj}}{\sum_{j \in [1,N_g]} \varepsilon_{gj}} \tag{6}$$

where the left-hand side term represents internal energy of the particle. On the right-hand side, the first term is heat conduction for the particle phase, the second term denotes heat of the pyrolysis reaction, the third term is total energy of the pyrolysis gas, the fourth term represents thermal convection, the fifth term is associated with effective heat diffusion flow and the sixth term is the dissipative phase. q_{gp} is the heat transfer of the gas flowing through the particle surface, h, λ and Q_g is the specific enthalpy (J · kg^{-1}), thermal conductivity (W · m^{-1} · K^{-1}), effective heat diffusion flux (W · m^{-2}), and $\underline{\underline{\mathbf{K}}}$ is permeability tensor (m^2). The conservation of the gas phase in the porous zone can be expressed as follows,

$$\partial_t (\varepsilon_g \rho_g) + \partial_{\mathbf{x}} \cdot (\varepsilon_g \rho_g \boldsymbol{u_g}) = S_g \tag{7}$$

where S_g is the generation rate of pyrolysis gas (kg · m^{-3} · s^{-1}).

$$S_g = \sum_{i \in [1,P_i]} \varepsilon_{si} \rho_s \partial_t \chi_i \tag{8}$$

$$\sum_{j \in [1,N_g]} \varepsilon_{gj} + \sum_{i \in [1,N_p]} \varepsilon_{si} = 1 \tag{9}$$

In the region of the porous media, the gas phase obeys Darcy's law with Klingberg's correction factor expressed as follows,

$$\boldsymbol{u_g} = -\frac{1}{\varepsilon_g} \left(\frac{1}{\mu} \underline{\underline{\mathbf{K}}} + \frac{1}{p} \underline{\underline{\beta}} \right) \cdot \partial_{\mathbf{x}} p \tag{10}$$

where ε_g is the porosity, $\boldsymbol{u_g}$ is the gas velocity (m · s^{-1}), $\underline{\underline{\beta}}$ is the Klinkenberg correction factor (Pa), and P is the pressure (Pa).

2.2. Conservation equation of gas phase

In the gas flow region outside the particle, the water vapor generated by water evaporation, the volatile generated by pyrolysis, and the heating gas entering the inlet were mixed and then flowed out of the calculation area from the outlet. When gas flowed through the surface of particles, heat transfer occurred between the gas and particles due to the temperature difference between the gas and the particle surface, the conservation equations for the gas phase are as follows,

$$\partial_t (\rho_g \boldsymbol{u_g} \cdot \boldsymbol{u_g}) + \partial_{\mathbf{x}} \cdot (\rho_g \boldsymbol{u_g} \cdot \boldsymbol{u_g}) = -\partial_{\mathbf{x}} p + \partial_{\mathbf{x}} \cdot \tau \tag{11}$$

$$\tau = \mu \left[(\partial_{\mathbf{x}} \boldsymbol{u_g} + \partial_{\mathbf{x}} \boldsymbol{u_g}^T) - \frac{2}{3} \partial_{\mathbf{x}} \cdot (\boldsymbol{u_g} \mathbf{I}) \right] \tag{12}$$

$$\partial_t (\rho_g c_g T_g) + \partial_x (\rho_g \boldsymbol{u_g} c_g T_g) = \partial_x (\lambda_g \partial_x T_g) + q_{pg} \tag{13}$$

$$\partial_t\left(\rho_g\varepsilon_{gj}\right) + \partial_x \cdot \left(\rho_g\boldsymbol{u_g}\varepsilon_{gj}\right) = \partial_x\mu_{eff} \cdot \partial_x Y_j + \dot{R}_j \tag{14}$$

where μ_{eff} is the dynamic viscosity (Pa$\cdot$s^{-1}), Y_j denotes the mass fraction of the gas phase component j (volatile and N$_2$).

2.3. Pyrolysis equation

During the simulation process, biomass is simplified as consisting of cellulose, hemicellulose, and lignin [26]. The results of elemental analysis and chemical composition analysis are shown in Table 1.

$$\frac{\partial_t\chi_i}{(1-\chi_i)} = A_i\exp\left(-\frac{E_i}{RT}\right), i \in \left[1, N_p\right] \tag{15}$$

where E_i is the activation energy of the component during pyrolysis (J$\cdot$kg^{-1}), A_i is pre-exponential factor and N_p is total number of components. The detailed parameters are presented in Table 2.

The equation of water evaporation is as follows [31],

$$\text{water}\xrightarrow{k_w}\text{water vapour} \tag{16}$$

Equation (16) is simulated by the Arrhenius formula, in which the exponential factor and the activation energy are $A = 5.13 \times 10^6$ s^{-1} and $E = 88000$ Kg$\cdot$m$^2\cdot$s$^{-2}\cdot$K^{-1}, respectively.

2.4. Computational model

The computational model is shown in Fig. 1. The biomass particle is initially spherical, and the heating gas flows over the particle from left to right. Heat is transferred from the heating gas to the particle by convective heat transfer, and the temperature of the particle gradually increases, then the pyrolysis reaction takes place and the diameter of the particle gradually decreases. After the volatile components have volatilized, the remaining solid phase forms charcoal.

The main parameters used in the simulation are shown in Table 3.

First, a preliminary study is performed to facilitate the choice of the appropriate grid resolution. Fig. 2 shows the central point temperature of a particle at different grid resolutions. The numerical simulations for resolutions 13000 and 43875 are very similar. Both simulations show the process of the particle's central point temperature gradually increasing with time. However, for grid numbers 1625 and 6656, there is temperature variation. Therefore, we choose the average grid resolution of 13000 for the present simulations.

3. Results and discussion

3.1. Model validation

Figs. 3 and 4 show the time variation of the simulated weight loss rate of the particles and their core temperature. According to Ref. [32], the diameter of the biomass particles is 20 mm, the pyrolysis atmosphere is nitrogen, and the heating temperature is 773 K. It can be seen that the pyrolysis process can be mainly divided into a heating stage before pyrolysis, a fast pyrolysis stage, and another heating stage after pyrolysis. At about 50 s, the temperature increases to 500 K and pyrolysis begins. The core temperature of the particles reaches 560 K at 180 s. During this time most of the volatile components in the particles have been devolatilized. At 240s, the core temperature of the particles is 610 K and the pyrolysis process is essentially complete. Without the intra-particle conduction, the pyrolysis starts with a certain delay. Fig. 4 also shows the temperature rise rate of the particle center. In the heating stage before pyrolysis, the temperature rise rate of the particle center is higher without intra-particle conduction, for the synchronous increase in temperature throughout the particle When pyrolysis begins, the heat absorbed by the particles is partially used to provide pyrolysis. The particle center reaches the pyrolysis temperature earlier without intra-particle conduction, resulting in a slower temperature rise rate, which is lower than the temperature rise rate with intra-particle conduction. The simulation results agree better with the experimental measurements when the heat conduction within the particles is taken into account.

Table 1
Ultimate analysis and composition of biomass [27].

Ultimate analysis (%)				Composition (%)			
C	H	O		Cellulose	Hemicellulose	Lignin	Water
62.4	5.6	32		42.75	26.325	20.925	10

The pyrolysis rate can be calculated as follows.

Table 2
Kinetic equation of pyrolysis [28–30].

Pyrolysis equation			A	E	γ
$(1-\gamma_1)$volatiles+			$A_1 = 7.94 \times 10^{16}$	$E_1 = 195000$	$\gamma_1 = 0.56$
hemicellulose$\overset{k_1}{\rightarrow}$	$(1-\gamma_2)$volatiles		$A_2 = 1.26 \times 10^7$	$E_2 = 96000$	$\gamma_2 = 0.45$
γ_1 intermediate solid	$\overset{k_2}{\rightarrow}$	$+$ $\gamma_2$char			
cellulose$\overset{k_C}{\rightarrow}(1-\gamma_C)$volatiles$+\gamma_C$char			7.94×10^{16}	202650	0.75
lignin$\overset{k_l}{\rightarrow}(1-\gamma_l)$volatiles$+\gamma_l$char			5.09×10^5	95000	0.66
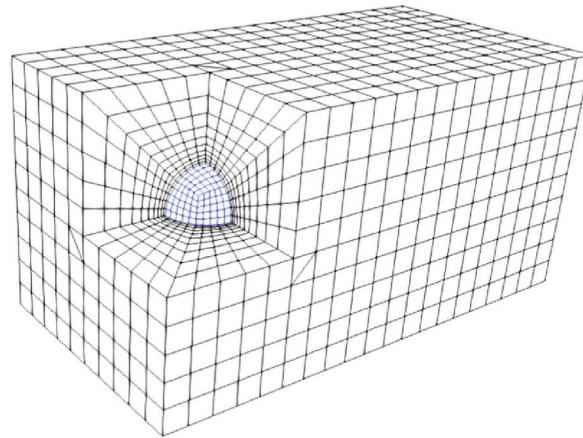
Fig. 1. Schematic diagram of geometric model.

Table 3
Physical parameters used for simulations.

Parameter	Simulation data	Unit
Specific heat of raw material, $c_{p,w}$	$2300 - 1150\exp(-0.0055T)$	$J \cdot kg^{-1} \cdot K^{-1}$
Specific heat of char, $c_{p,c}$	$1430 + 0.36T - 7.320^7 T^{-2}$	$J \cdot kg^{-1} \cdot K^{-1}$
Thermal conductivity of raw material, λ_w	$0.291 + 0.000836 \times 0.33T$	$W \cdot m^{-1} \cdot K^{-1}$
Thermal conductivity of char, λ_c	$2.36 - 1.50 \times 10^{-2} \times T + 3.85^{10} - 5 \times T^2 - 4.33 \times 10^{-8} \times T^3 + 1.86 \times 10^{-11} \times T^4$	$W \cdot m^{-1} \cdot K^{-1}$
Thermal conductivity, λ_g	$770 + 0.63T + 0.00019T^2$	$W \cdot m^{-1} \cdot K^{-1}$
Viscosity, μ	3×10^{-5}	$Kg \cdot m^{-1} \cdot K^{-1}$
Number of grid elements	13000	

3.2. Heat transfer and reaction characteristics of particles during pyrolysis

Fig. 5 illustrates the radial temperature variation inside the particle along the gas flow direction during the pyrolysis process. There is a clear temperature gradient inside the particle, and the temperature initially increases in the direction of the incoming gas. The dotted line in Fig. 5 represents the initial geometry of the particle. The region facing the incoming flow pyrolyzes first, resulting in rapid shrinkage in the volume of the particles. Due to the different temperature rise rates and pyrolysis rates at different positions in the particles, the shape of the particles also changed. At the end of the reaction, the particle deforms back to an approximately spherical shape. Fig. 6 shows the variation of temperature at five different locations inside the particle along the diameter. Throughout the process, a large temperature difference can be observed inside the particle. Among the different points, the fastest temperature rise is observed at the point (a) in the direction of the incoming flow, followed by the adjacent point (b). The temperature rise is lowest near point (d) on the leeward side of the particle. Initially, the temperature at the central point (c) is lower than the temperature at point (e) on the leeward side. However, due to the strong convective heat transfer and significant heat exchange at point (e), the temperature there rises faster and after a while exceeds the temperature at point (c). The maximum temperature difference inside the particle is 146.7 K at 30s, 122.7 K at 60s, and 125.0 K at 90s. The internal temperature distribution of the particle tends to uniformity at the end of the reaction.

Fig. 7 illustrates the relationship between the remaining mass and the original mass of the biomass particles. Also shown is the ratio of the remaining mass of each component to the original mass of that component at a particular point in the pyrolysis process. It can be seen that the pyrolysis rate of hemicellulose is the fastest and mainly occurs in the temperature range of 500–625 K. This is followed by
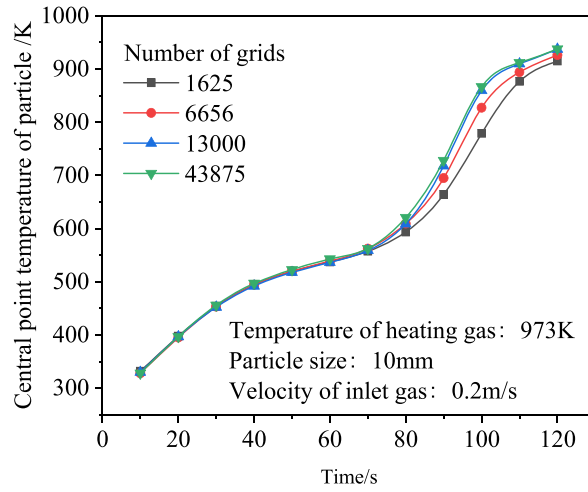
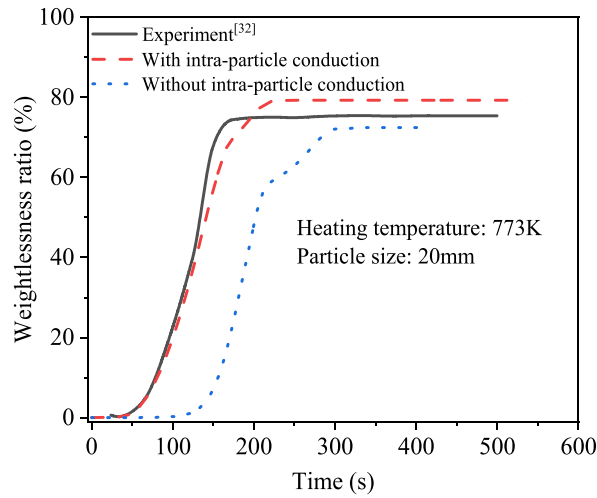**Fig. 2.** Central point temperature of the particles at different grids.

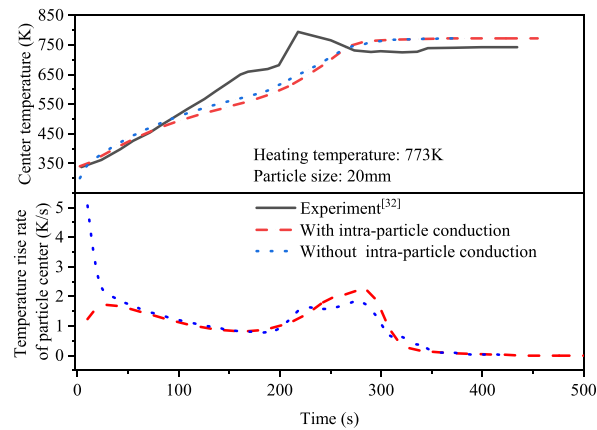**Fig. 3.** Weightlessness ratio of particle.

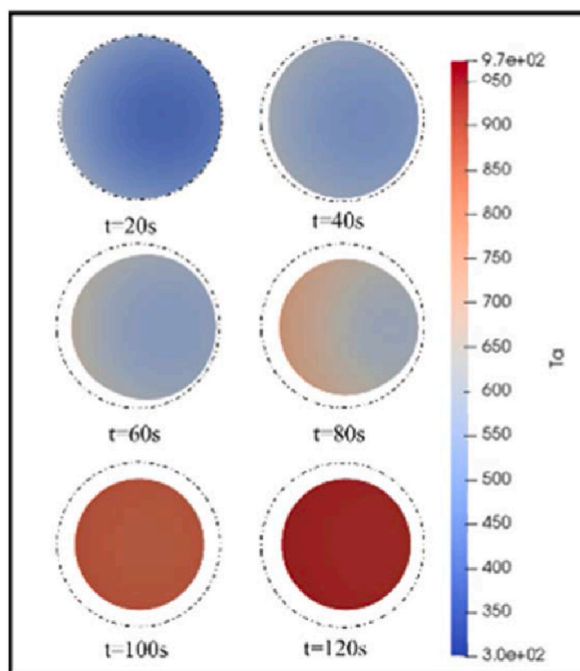**Fig. 4.** Temperature change of particle center.

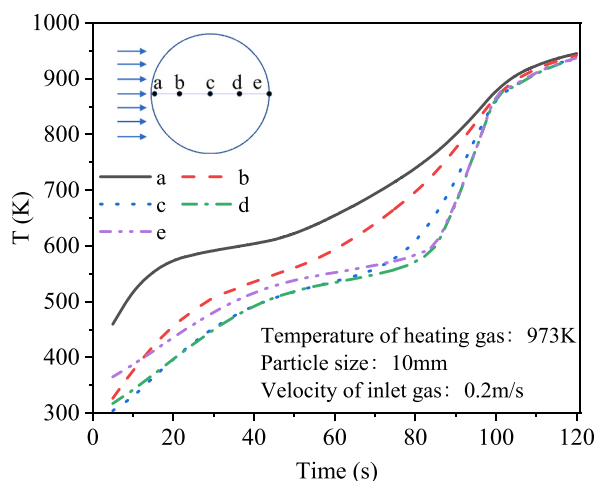**Fig. 5.** Temperature distribution at a cross-section inside the particle.

Fig. 6. Variations of temperature at different positions inside the particle.

cellulose with the main pyrolysis range of 550K–675 K and lignin with the slowest pyrolysis process, which mainly occurs in the range of 600K–875 K, which is consistent with Park's research results [10]. Combining Figs. 6 and 7, it can be seen that at a temperature between 500 and 600 K, the temperature of the particles increases slowly and the mass of the particles decreases rapidly.

Figs. 8 and 9 show the variations of particle surface temperature and average particle temperature and particle mass and size with time. The particle surface temperature refers to the average of temperature over the entire surface. The heat released by the particles gradually increases their temperature and triggers the decomposition of the biomass particles. Compared with the results without the internal heat conduction of particles, the average temperature of particles is always lower during the pyrolysis process, and the surface temperature of particles is higher at the beginning, then the heating rate decreases due to the pyrolysis reaction. When the heat conduction inside the particles is considered, the heat absorbed by the particles is gradually transferred from the surface to the interior. The surface of the particles first reaches the pyrolysis reaction temperature and starts to pyrolyze, and the mass gradually decreases. When the particle internal heat conduction is not considered, the pyrolysis of the whole particle starts quickly when the particle temperature reaches the pyrolysis temperature, and the pyrolysis time is shorter than when the particle internal heat conduction is considered.
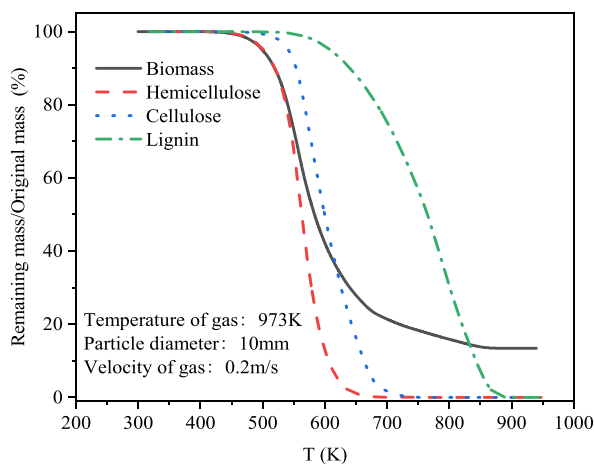
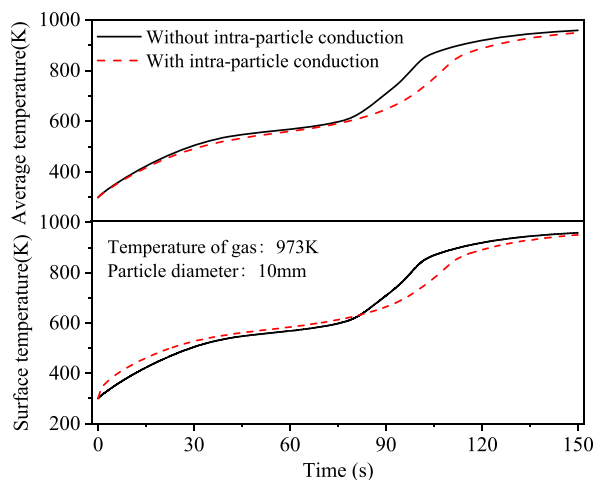**Fig. 7.** The residual mass fraction of each component.

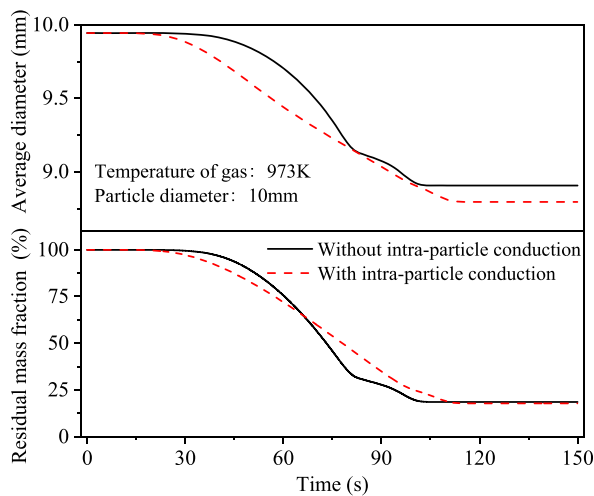**Fig. 8.** Variation of particle temperature.

Fig. 9. Variation of particle mass and size.

During the pyrolysis process, the heat absorbed by the particles is provided by convective heat transfer from the gas phase. The absorbed heat is used for heating the particles and pyrolysis. At the same time, some of the heat is removed from the particles by the volatilization of the pyrolysis due to Stephen flow [33], and the energy balance equation is as follows

$$\overline{H} \cdot A \cdot (T_\infty - T_s) = m_s c_{Ps}(T_{s2} - T_{s1}) + R_{heat} + \dot{m}_s c_{Pg} T_s \tag{17}$$

where $\overline{H}$ is the average convective heat transfer coefficient between the fluid and the particle surface ($W\,m^{-2}\,K^{-1}$). T_∞ is the fluid temperature (K), T_s is the average particle surface temperature (K), and A is the particle surface area (m^2), $\dot{m}_s$ is the biomass reaction rate (kg/s). The Nusselt number (Nu) is defined as follows:

$$Nu = \frac{\overline{H} \cdot d}{\lambda} \tag{18}$$

Fig. 10 shows the change in Nusselt number with time according to Equation (18). The Nusselt number calculated by heating the particles only, without pyrolysis, is essentially the same as the Nusselt number calculated by the empirical formula. Fig. 10 also shows the heat absorption due to the temperature rise of the particles, moisture evaporation and pyrolysis of the three organic components during the pyrolysis process. At the beginning of the pyrolysis reaction, the Nusselt number increases because the heat absorbed by the particles is mainly used for the evaporation of water and the pyrolysis of cellulose and hemicellulose, which delays the increase of particle temperature. When the pyrolysis of cellulose and hemicellulose is almost complete, the heat absorbed by the particle continues to be used for the temperature rise, and the Nusselt number decreases. At about 90 s, lignin begins to decompose. As the lignin pyrolysis rate increases, the Nusselt number increases. At the end of the pyrolysis reaction, the Nusselt number decreases again and is slightly lower than the Nusselt number calculated with the empirical formula.

3.3. Influence of moisture content

Figs. 11 and 12 show the effects of moisture content on particle temperature and residual mass, respectively. In the calculation, the mass of organic matter in the particles and the diameter of the particles are kept unchanged, and the total density of the particles increases with increasing moisture content. Since heat is required to evaporate the moisture, the higher the moisture content, the slower the temperature of the particles increases. In addition, the effect of moisture content on the heating rate is more pronounced at the center (c) and leeward (e) sides of the particles than at the windward (a). A higher moisture content results in a longer time to complete the pyrolysis process. The time required to complete pyrolysis at a moisture content of 15 % is about 50 s higher than in the case without water.

Fig. 13 shows the effects of moisture content on Nusselt number. As the moisture content increases, the temperature rise of the particles decreases and the first peak of the Nusselt number increases. Increasing the moisture content increases the reaction time of pyrolysis. When pyrolysis of lignin starts, the average total temperature of the particles is higher due to the longer reaction time, and the temperature rise is relatively small, so the difference between the two peaks of the Nusselt number decreases.

3.4. Influence of particle size

Figs. 14 and 15 illustrate the effects of particle size on temperature and residual mass, respectively. As particle size increases, the time required to heat the particles and complete pyrolysis increases. In addition, the temperature difference between the center of the particles and their surface increases. At 970 K, the time required for the temperature rise of particles with a diameter of 20 mm is about 15 times higher than that of particles with a diameter of 2 mm, and the corresponding pyrolysis time is about 20 times longer. The larger the particle size, the greater the difference between the temperature at the center of the particles and the surface temperature. The disparity is attributed to the fact that larger particle sizes must overcome greater thermal resistance during heat conduction, which diminishes the rate of temperature increase at the center of particles. Conversely, reduced surface area leads to a more rapid rise in surface temperature. These factors are crucial for regulating and optimizing pyrolysis processes involving large biomass particles. In addition to the heat transfer factor, another reason for the decrease in pyrolysis rate with increasing particle size is that volatile products must diffuse from inside the particle to its surface before being released into the surrounding environment. For the larger particles, this diffusion distance increases, resulting in greater resistance and a slower decline in residual mass fraction.

Fig. 16 shows the effect of particle size on the Nusselt number. It can be observed that the variation of Nusselt number shows a similar trend for different particle sizes during the pyrolysis process. As the particle size increases, the difference between the two peak values decreases and the time interval between the two peak values increases. When the particle diameter is 2 mm, the two peak values of Nusselt number are 5.7 and 13.2, respectively, and the time interval is about 4 s. When the particle diameter is 10 mm, the two peak values are 8.2 and 10.5, respectively, and the time interval is about 15 s. When the particle diameter is 20 mm, the two peak values are very close and the time interval is about 30 s. During the initial stage of pyrolysis, surface reactions dominate and result in higher reaction rates on larger biomass particles. The reaction products are quickly diffused out, leading to a significant peak in the Nusselt number. However, as the reaction progresses into later stages, larger particle sizes lead to smaller specific surface areas and slower heat and mass transfer rates, resulting in a lower peak Nusselt number.
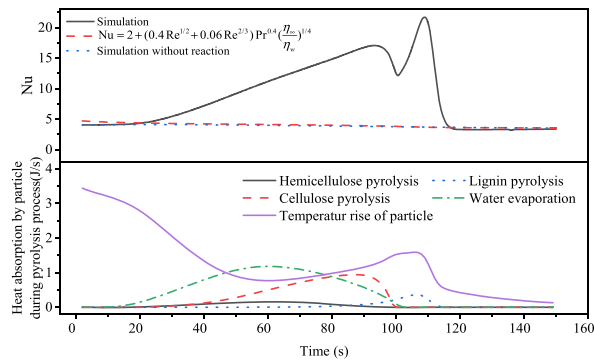
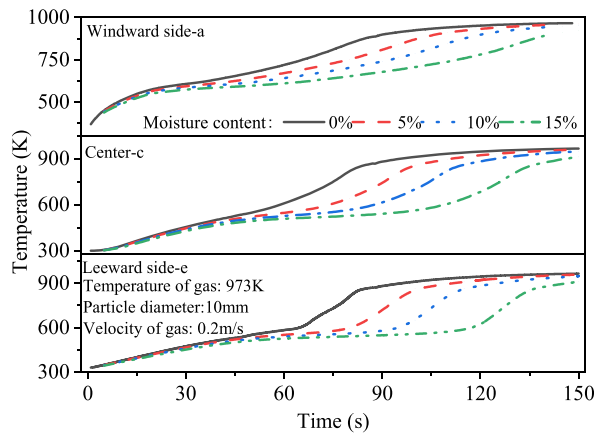**Fig. 10.** Temporal variation of *Nu* on the particle surface.

Fig. 11. Influence of moisture content on particle temperature.
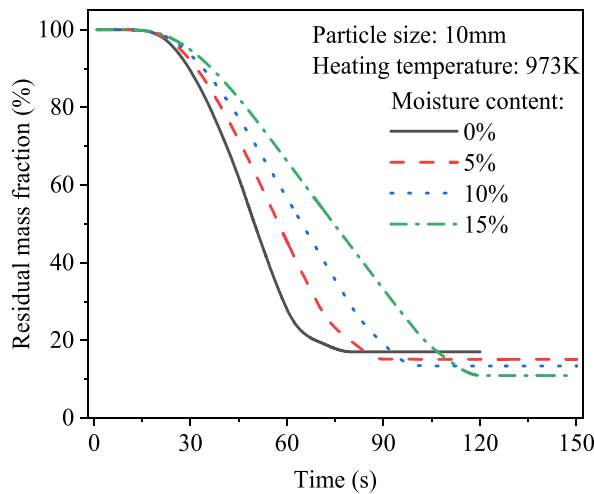

Fig. 12. Influence of moisture content on particle residual mass fraction.

3.5. Influence of gas velocity

Figs. 17 and 18 show the influence of the gas velocity on the temperature distribution of the particles and the residual mass fraction, respectively. The higher the gas velocity, the faster the temperature of the particles rises at different positions in the particles, the earlier the pyrolysis begins, and the shorter the time required for completion of the pyrolysis. The higher the gas velocity at the
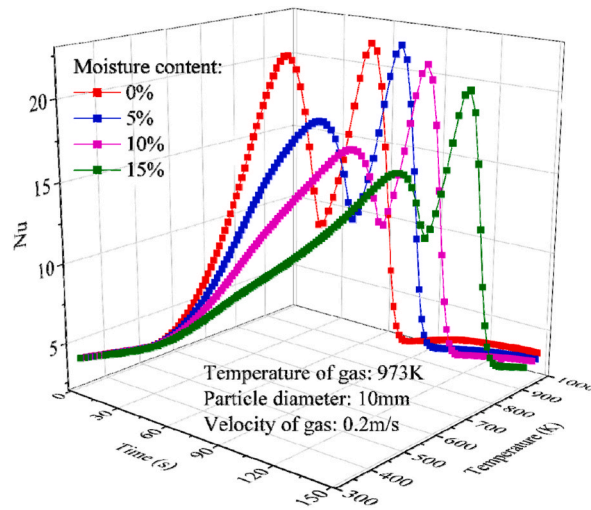
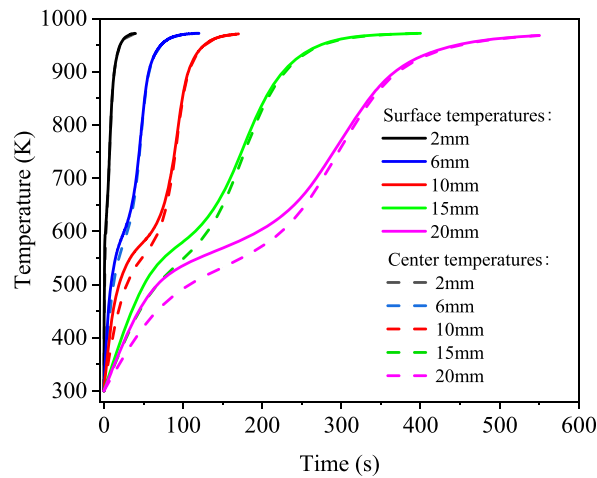**Fig. 13.** Influence of moisture content on the Nusselt number.

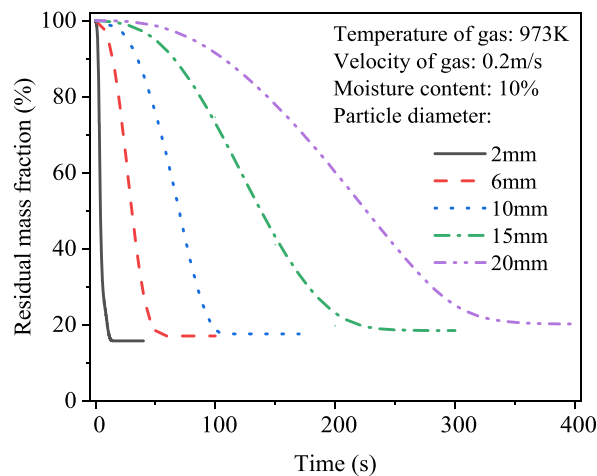**Fig. 14.** Influence of particle size on temperature.

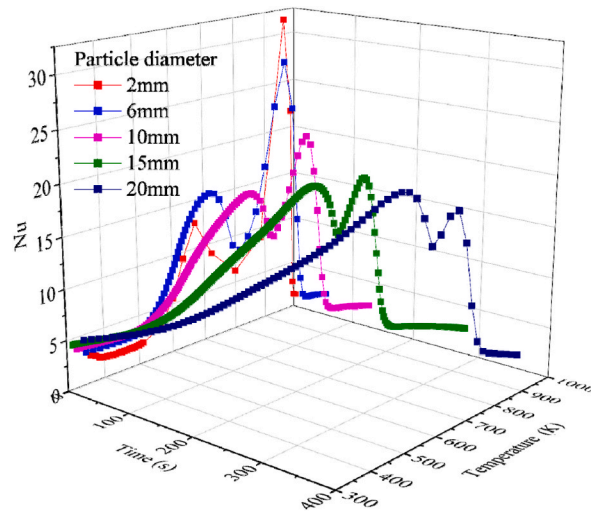**Fig. 15.** Influence of particle size on residual mass fraction.

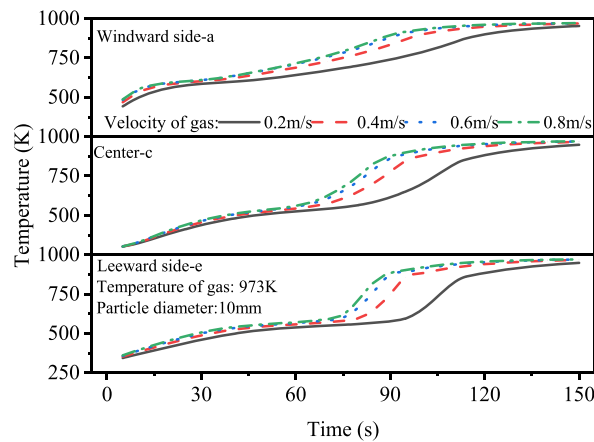**Fig. 16.** Influence of particle size on *Nu*.

Fig. 17. Influence of gas velocity on temperature.
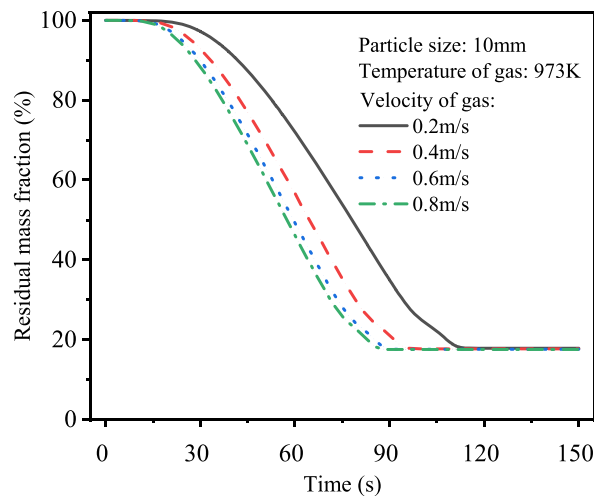

Fig. 18. Influence of gas velocity on residual mass fraction.

beginning, the greater the temperature difference between point a of the particle surface and point c of the particle center. At a gas velocity of 0.2 m/s, the temperature difference between point a and point c is 173 K after 10 s, and at a gas velocity of 0.8 m/s, the temperature difference is 218 K. As time increases, the surface of the particles gradually begins to pyrolyze, and the temperature difference between a point and the c point decreases. The higher the gas velocity, the faster the temperature difference drops. This is because the higher the gas velocity, the higher the surface temperature of the particles, and the more intense the pyrolysis reaction. At 45 s, the temperature difference between point a and point c is 120 K at a gas velocity of 0.2 m/s, and at a gas velocity of 0.8 m/s, the temperature difference is 130 K. In the later stage of the pyrolysis reaction, the decomposition of the particle surface is completed, the decomposition of the particle interior begins gradually, and the temperature difference between the particle surface and particle interior increases. The temperature difference between point a and point c is 135 K when the gas velocity is 0.2 m at 85 s, and 153 K when the velocity is 0.8 m/s at 65 s. At the end of the reaction, the temperature difference between the surface and the interior of the particles gradually decreases. At a gas velocity of 0.2 m/s, the temperature difference between point a and point c is 25 K, and at a velocity of 0.8 m/s, the temperature difference is 7 K. At the four different gas velocities, the times for the residual mass of the particles to reach 20 % are 108s, 91s, 85s and 82s respectively.

Fig. 19 shows the effect of gas velocity on Nu. Increasing the gas velocity improves the heat transfer between the gas and the particle surface, and Nu ncreases. Although the gas velocity is different, the particle temperature corresponding to the maximum value of Nu is relatively low. The particle temperature corresponding to the first peak value of Nu is 670–680 K, and the particle temperature corresponding to the second peak value of Nu is 820–840 K. As the gas velocity increases, the occurrence of the peak value is delayed, the difference between the two peak values increases, and the time between the two peak values decreases slightly. The effect of gas velocity on heat transfer enhancement decreases with increasing gas velocity. The Nu is very close when the gas velocity is 0.6 m/s and 0.8 m/s. This is because the high gas velocity causes a vortex at the end of the particle, which affects the contact between the particle and the high temperature gas, thus affecting the heat transfer efficiency.

4. Conclusions

In this work, a numerical model for the pyrolysis of a single biomass particle was established, taking into account the internal conduction of large particles in the pyrolysis. Accordingly, the internal temperature distribution of the particle and the heat transfer characteristics during the pyrolysis process were determined.

(1) The temperature distribution and composition were different in different places inside the particle. The maximum temperature difference inside the particle was about 146.7 K when the particle diameter was 10 mm.
(2) The temperature increased rapidly along the flow direction, leading to an earlier onset of pyrolysis and a change in particle shape. During the pyrolysis process, there were two peaks of Nusselt number.
(3) The increase of moisture content prolonged the reaction time of pyrolysis. The pyrolysis time of particles with moisture content of 15 % was about 1.5 times longer than that of dry particles when the particle diameter was 10 mm.
(4) As the particle size increased, the temperature difference between the surface and the center of the particles increased, resulting in a longer pyrolysis time. The difference between the two peaks decreased and the time interval between the two peaks increased.
(5) Increasing the gas velocity improves the heat transfer between the gas and the particle surface, and the effect of the gas velocity on improving the heat transfer is limited when the gas velocity is too high.
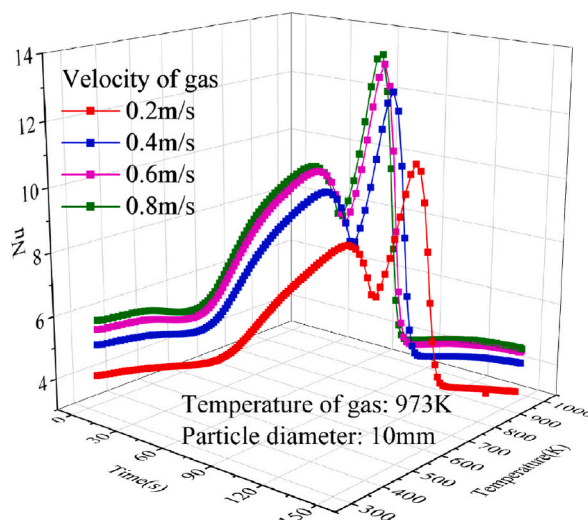

Fig. 19. Influence of the gas velocity on Nu.

Data availability statement

The data used to support the findings of this study are available from the corresponding author upon request.

CRediT authorship contribution statement

H.A.N. Fei-yang: Data curation, Writing – original draft. **W.A.N.G. Meng:** Data curation. **M.A. Xiao-bo:** Supervision. **Li-jie Yin:** Data curation, Writing – original draft, Writing – review & editing. **De-zhen Chen:** Supervision, Writing – review & editing. **L.I.U. Ze-qing:** Investigation, Supervision. **Z.H.A.N.G. Rui-na:** Investigation, Supervision.

Declaration of competing interest

The authors declare that they have no known competing financial interests or personal relationships that could have appeared to influence the work reported in this paper.

Acknowledgements

References

[1] P. Kumar, P.M.V. Subbarao, L.D. Kala, V.K. Vijay, Thermogravimetry and associated characteristics of pearl millet cob and eucalyptus biomass using differential thermal gravimetric analysis for thermochemical gasification, Therm. Sci. Eng. Prog. 26 (2021), 101104, https://doi.org/10.1016/j.tsep.2021.101104.

[2] L.Q. Lu, X. Gao, J.F. Dietiker, M. Shahnam, W.A. Rogers, MFiX based multi-scale CFD simulations of biomass fast pyrolysis: a review, Chem. Eng. Sci. 248 (2022), 11713.

[3] B. Li, Y. Ge, C. Xu, J. Shi, M. Chen, S. Geng, C. Cheng, Research on the coordinated and sustainable development of jiangsu power grid under the "double carbon" goal, IOP Conf. Ser. Earth Environ. Sci. 772 (1) (2021), 012019, https://doi.org/10.1088/1755-1315/772/1/012019.

[4] T.M. Ismail, M. Abd El-Salam, M.A. El-Kady, S.M. El-Haggar, Three dimensional model of transport and chemical late phenomena on a MSW incinerator, Int. J. Therm. Sci. 77 (2014) 139–157, https://doi.org/10.1016/j.ijthermalsci.2013.10.019.

[5] Q. Xiong, S.C. Kong, High-resolution particle-scale simulation of biomass pyrolysis, ACS Sustain. Chem. Eng. 4 (10) (2016) 5456–5461, https://doi.org/10.1021/acssuschemeng.6b01020.

[6] D. Chen, L. Yin, H. Wang, P. He, Pyrolysis technologies for municipal solid waste: a review, Waste Manag. 34 (12) (2014) 2466–2486, https://doi.org/10.1016/j.wasman.2014.08.004.

[7] H. Lu, E. Ip, J. Scott, P. Foster, M. Vickers, L.L. Baxter, Effects of particle shape and size on devolatilization of biomass particle, Fuel 89 (5) (2010) 1156–1168, https://doi.org/10.1016/j.fuel.2008.10.023.

[8] F. Buss, S. Wirtz, V. Scherer, Simulation of a reacting agitated bed of straw pellets by a resolved coupled DEM/CFD method using a blocked-off approach, Int. J. Therm. Sci. 152 (2020), 106332, https://doi.org/10.1016/j.ijthermalsci.2020.106332.

[9] C. Di Blasi, Heat, momentum and mass transport through a shrinking biomass particle exposed to thermal radiation, Chem. Eng. Sci. 51 (7) (1996) 1121–1132, https://doi.org/10.1016/S0009-2509(96)80011-X.

[10] W.C. Park, A. Atreya, H.R. Baum, Experimental and theoretical investigation of heat and mass transfer processes during wood pyrolysis, Combust. Flame 157 (3) (2010) 481–494, https://doi.org/10.1016/j.combustflame.2009.10.006.

[11] H. Luo, X. Wang, X. Liu, X. Wu, X. Shi, Q. Xiong, A review on CFD simulation of biomass pyrolysis in fluidized bed reactors with emphasis on particle-scale models, J. Anal. Appl. Pyrol. 162 (2022), 105433, https://doi.org/10.1016/j.jaap.2022.105433.

[12] F. Qi, M.M. Wright, A DEM modeling of biomass fast pyrolysis in a double auger reactor, Int. J. Heat Mass Tran. 150 (2020), 119308, https://doi.org/10.1016/j.ijheatmasstransfer.2020.119308.

[13] F. Qi, M.M. Wright, Particle scale modeling of heat transfer in granular flows in a double screw reactor, Powder Technol. 335 (2018) 18–34, https://doi.org/10.1016/j.powtec.2018.04.068.

[14] H. Luo, X. Wang, X. Liu, L. Yi, X. Wu, X. Yu, Y. Ouyang, W. Liu, Q. Xiong, Machine learning based prediction of biomass pyrolysis with detailed reaction kinetics for thermally-thick particles: from 1D to 0D, Chem. Eng. Sci. 280 (2023), 119060, https://doi.org/10.1016/j.ces.2023.119060.

[15] L. von Berg, A. Soria-Verdugo, C. Hochenauer, R. Scharler, A. Anca-Couce, Evaluation of heat transfer models at various fluidization velocities for biomass pyrolysis conducted in a bubbling fluidized bed, Int. J. Heat Mass Tran. 160 (2020), 120175, 10.1016/j.ijheatmasstransfer. 2020.120175.

[16] P.N. Ciesielski, M.F. Crowley, M.R. Nimlos, A.W. Sanders, G.M. Wiggins, D. Robichaud, B.S. Donohoe, T.D. Foust, Biomass particle models with realistic morphology and resolved microstructure for simulations of intraparticle transport phenomena, Energy & Fuels 29 (1) (2015) 242–254, 10.1021/ef502204v.

[17] D. Meng, T. Wang, J. Xu, X. Chen, A numerical study on the pyrolysis of large coal particles: heat transfer and volatile evolution, Fuel 254 (2019), 115668, https://doi.org/10.1016/j.fuel.2019.115668.

[18] M.G. Nugraha, H. Saptoadi, M. Hidayat, B. Andersson, R. Andersson, Particle modelling in biomass combustion using orthogonal collocation, Appl. Energy 255 (2019), 113868, https://doi.org/10.1016/j.apenergy.2019.113868.

[19] H. Luo, X. Wang, X. Wu, L. Niedzwiecki, H. Pawlak-Kruczek, X. Liu, Q. Xiong, Multi-fluid modeling of heat transfer in bubbling fluidized bed with thermally-thick particles featuring intra-particle temperature inhomogeneity, Chem. Eng. J. 460 (2023), 141813, https://doi.org/10.1016/j.cej.2023.141813.

[20] M. Mohseni, B. Peters, M. Baniasadi, Conversion analysis of a cylindrical biomass particle with a DEM-CFD coupling approach, Case Stud. Therm. Eng. 10 (2017) 343–356, https://doi.org/10.1016/j.csite.2017.08.004.

[21] X. Li, C. Yin, S. Knudsen Kær, T. Condra, A detailed pyrolysis model for a thermally large biomass particle, Fuel 278 (2020), 118397, https://doi.org/10.1016/j.fuel.2020.118397.

[22] I. Wardach-Święcicka, D. Kardaś, Modelling thermal behaviour of a single solid particle pyrolysing in a hot gas flow, Energy 221 (2021), 119802, https://doi.org/10.1016/j.energy.2021.119802.

[23] A.M.C. Janse, R.W.J. Westerhout, W. Prins, Modelling of flash pyrolysis of a single wood particle, Chem. Eng. Process: Process Intensif. 39 (3) (2000) 239–252, https://doi.org/10.1016/S0255-2701(99)00092-6.

[24] G. Caposciutti, H. Almuina-Villar, A. Dieguez-Alonso, T. Gruber, J. Kelz, U. Desideri, C. Hochenauer, R. Scharler, A. Anca-Couce, Experimental investigation on biomass shrinking and swelling behaviour: particles pyrolysis and wood logs combustion, Biomass Bioenergy 123 (2019) 1–13, https://doi.org/10.1016/j.biombioe.2019.01.044.

[25] L. Terrei, Z. Acem, V. Marchetti, P. Lardet, P. Boulet, G. Parent, In-depth wood temperature measurement using embedded thin wire thermocouples in cone calorimeter tests, Int. J. Therm. Sci. 162 (2021), 106686, https://doi.org/10.1016/j.ijthermalsci.2020.106686.

[26] P. Rahimi Borujerdi, B. Shotorban, S. Mahalingam, D.R. Weise, Modeling of water evaporation from a shrinking moist biomass slab subject to heating: Arrhenius approach versus equilibrium approach, Int. J. Heat Mass Tran. 145 (2019), 118672, 10.1016/j.ijheatmasstransfer. 2019. 118672.

[27] E. Biagini, F. Barontini, L. Tognotti, Devolatilization of biomass fuels and biomass components studied by TG/FTIR technique, Ind. Eng. Chem. Res. 45 (13) (2006) 4486–4493, https://doi.org/10.1021/ie0514049.

[28] G. Varhegyi, M.J. Antal, T. Szekely, P. Szabo, Kinetics of the thermal decomposition of cellulose, hemicellulose, and sugarcane bagasse, Energy & Fuels 3 (3) (1989) 329–335, https://doi.org/10.1021/ef00015a012.

[29] R.W.-C. Chan, B.B. Krieger, Kinetics of dielectric-loss microwave degradation of polymers: lignin, J. Appl. Polym. Sci. 26 (5) (1981) 1533–1553, https://doi.org/10.1002/app.1981.070260510.

[30] R. Capart, L. Khezami, A.K. Burnham, Assessment of various kinetic models for the pyrolysis of a microgranular cellulose, Thermochim. Acta 417 (1) (2004) 79–89, https://doi.org/10.1016/j.tca.2004.01.029.

[31] V. Pozzobon, S. Salvador, J.J. Bézian, M. El-Hafi, Y. Le Maoult, G. Flamant, Radiative pyrolysis of wet wood under intermediate heat flux: experiments and modelling, Fuel Process. Technol. 128 (2014) 319–330, 10.1016/j.fuproc.2014.07.007.

[32] K. Wang, H. Zhang, S. Chu, Z. Zha, Pyrolysis of single large biomass particle: simulation and experiments, d, Chin. J. Chem. Eng. 29 (2021) 375–382, 10.1016/j.cjche.2020.09.032.

[33] K. Zhou, J. Yu, W.J.E. Ou, Fuels, Effects of Stefan flow on ignition and heat transfer of a char particle in, O2/CO2 atmospheres 27 (6) (2013) 3454–3459, https://doi.org/10.1021/ef4003473.